The final publication is available at

https://doi.org/10.1016/j.chemosphere.2019.125677

Additional Information

Photoelectrocatalyzed degradation of organophosphorus pesticide fenamiphos using WO₃ nanorods as photoanode

Roselló-Márquez, G.[a]; Fernández-Domene, R.M. [a]; Sánchez-Tovar, R. [a,b]; García-Antón, J.[a*]

[a] Ingeniería Electroquímica y Corrosión (IEC), Instituto Universitario de Seguridad Industrial, Radiofísica y Medioambiental (ISIRYM), Universitat Politècnica de València, Camino de Vera s/n, 46022 Valencia, Spain. [*] *jgarciaa@iqn.upv.es*

[b]Departmento de Ingeniería Química, Universitat de València, Av de les Universitats, s/n, 46100 Burjassot, Spain

ABSTRACT

In this study, WO₃ nanostructures were synthesized by the electrochemical anodization technique to use them on the degradation of persistent organic compounds such as the pesticide fenamiphos. The acids electrolyte used during the anodization were two different: 1.5 M H_2SO_4 - 0.05 M H_2O_2 and 1.5 M CH_4O_3S - 0.05 M H_2O_2. Once the samples have been manufactured, they have been subjected to different tests to analyze the properties of the nanostructures. With Field Emission Scanning Electron Microscopy (FE-SEM) the samples have been examined morphologically, their composition and crystallinity has been studied through Raman Spectroscopy and their photoelectrochemical behaviour by Photoelectrochemical Impedance Spectroscopy (PEIS). Finally, degradation tests have been carried out using the technique known as photoelectrocatalysis (PEC). The conditions that were applied in this technique were a potential of 1 $V_{Ag/AgCl}$ and simulated solar illumination. The degradation process was monitored by UV-Visible and High-Performance liquid Chromatography (HPLC) to control the course of the experiment. The nanostructures obtained with 1.5 M CH_4O_3S - 0.05 M H_2O_2 electrolyte showed a better photoelectrochemical behaviour than nanostructures synthesized with 1.5 M H_2SO_4 - 0.05 M H_2O_2. The fenamiphos degradation was achieved at 2 hours of experiment and the intermediate formation was noticed at 1 hour of PEC experiment.

Keywords: Fenamiphos, photoelectrocatalysis, WO₃ nanostructures, pesticide, degradation.

1. INTRODUCTION

Fenamiphos is an organophosphorus pesticide used as an insecticide and specifically as a nematicide which was first registered in 1972 (Cáceres et al., 2010). This pesticide is employed at diverse steps of plant growth, such as pre-planting, sowing, pre-harvest and post-harvest in a huge variety of plants like pineapples, turf, tobacco, bananas, citrus fruits and other types of vegetables and cereals (Ou et al., 2010). It can be found it groundwater, rivers, land and air (Michael. A. Kamrin, 2010; Singh and Walker, 2006). Its adverse ecological repercussions are often attributed to its persistence in all medias. Fenamiphos is highly toxic orally, with LD_{50} values reported from 2 to 19 $mg \cdot kg^{-1}$ in rats and from 56 to 100 $mg \cdot kg^{-1}$ in guinea pigs (Kidd, H. and James, D. R., 1991). The inhalation toxicity of the pesticide is also high, with inhaled LC_{50} values reported in rats of 0.11 to 0.17 $mg \cdot L^{-1}$ (Budd and Young, 2006; Cáceres et al., 2008).

In recent years, it has been reported that many elimination processes such as membrane separation (Ghaemi et al., 2011; Mehta et al., 2015; Plakas and Karabelas, 2012), chemical coagulation (Chen et al., 2007; Saini and Kumar, 2016; Sarkar et al., 2007), adsorption (Moussavi et al., 2013; Vukčević et al., 2015; Yang et al., 2014) and bioremediation (Cycoń et al., 2013; Helbling, 2015) can be used to remove different kinds of pesticides. Apart from them, advanced oxidation processes (AOP) such as UV/H_2O_2, Electro-Fenton, ultrasound, UV/O_3 and photocatalysis (PC) have attracted the public interest due to the high efficiency of these process, the environmental conditions and their reasonable cost. (Golash and Gogate, 2012; Navarro et al., 2009; Rass-Hansen et al., 2007; Reddy and Kim, 2015).

Photocatalysis process (PC) is based on the transfer of charge through the interface formed between a semiconductor that acts as a catalyst and an aqueous solution containing the contaminant. Photocatalysis uses a catalyst that is sensitive to radiation, therefore, it is a photochemical transformation. Most of the catalysts used are semiconductor metal oxides, which are characterized by having a band gap that extends from the valence band, to the conduction band. When the catalyst receives the energy of a photon (hv) the excitation of an electron (e^-) in the catalyst is produced and it gains enough energy to change the level. At the same time a hole (h^+) is formed in the valence band.

These two species (electron-hole) form a pair on the surface of the catalyst, where they can recombine (producing a decrease in process efficiency) or participate in redox reactions with substances adsorbed on the surface of the catalyst. If this interaction is carried out in an aqueous environment, HO· radicals will be produced which then will oxidize the organic species (Maldonado et al., 2007; Paul et al., 2012).

However, the recombination of charge between the electron-hole pair takes place easily and to reduce it a constant polarization potential is applied to the anode that

promotes the extraction of e^-_{CB} photoinduced by the external electric circuit, thus producing an efficient separation of the pairs of e^-_{CB} / h^+_{VB}.

The prevention of charge recombination improves the photocatalytic efficiency of the anode by generating more holes and accelerating organic oxidation compared to PC. The useful life of the holes increases and they have more opportunities to oxidize the organic contaminants adsorbed on the surface (Daghrir et al., 2012). This new technique is known as photoelectrocatalysis (PEC).

Photoelectrocatalysis with the use of semiconductors is a highly encouraging technique due to its advantages that involve the transformation of pollutants into innocuous elements, environmental working conditions, low cost, etc(Watcharenwong et al., 2008).

Using an n-type semiconductor photoelectrode, the configuration of a PEC cell consists of a working photoanode and a counter electrode (for example, the Pt cathode) both immersed in the electrolyte. In PEC, the photocatalyst can be easily recovered after application and recycled for consecutive treatments. At the moment in which the photoanode is illuminated, the separation between the holes and the electrons is produced. The holes are the responsible for producing oxygen when they arrive at the photoanode/electrolyte interface, while the electrons produce hydrogen when they reach the counter electrode. In conclusion, the whole reaction includes three fundamental steps: 1) light absorption; 2) separation and transport charge carrier; 3) superficial chemical reactions (Xiao et al., 2015).

Tungsten oxide (WO_3) is one of those n-type metal oxides semiconductors which has attracted significant consideration as a result of its high chemical stability in a low pH, excellent electrical conductivity, non-photoelectric corrosion and its ability to absorb a reasonable fraction of the solar spectrum (Berger et al., 2006; Li et al., 2010; Santato et al., 2001; Tsuchiya et al., 2005). In the last ten years, the WO_3 has been widely investigated because of its extensive range of applications in photovoltaics (He and Yao, 2007; Zheng et al., 2010; Zhou et al., 2005), photoelectrocatalysis (Fraga et al., 2013; Georgieva et al., 2011; Guo et al., 2007; Liu et al., 2011, 2010) and water splitting (Bamwenda et al., 1999; Chakrapani et al., 2009; Enesca et al., 2007; Miller et al., 2006).

In the present work, the structural, morphological and photoelectrochemical properties of WO_3 nanostructures were evaluated to study the influence of the acid electrolyte used during their synthesis by anodization. They were formed using two different electrolytes (1.5 M H_2SO_4 and 0.05 M H_2O_2 or 1.5 M CH_4O_3S and 0.05 M H_2O_2) and then they were subjected to an annealing treatment (600°C and in air atmosphere). The properties were evaluated through Raman Spectroscopy, Field

Emission Scanning Electronic Microscopy (FESEM) and Photoelectrochemical Impedance Spectroscopy (PEIS).

The use of methanesulfonic acid (CH_4O_3S, MSA) in several fields such as catalysis, electrochemistry, esterification, etc. is due to the numerous physical and chemical properties that make it exceptional. These include its excellent solubilization of metal salts, characterized by being a strong acid with a pKa of 21.9 that is almost ionized in 0.1 M aqueous solutions (Gernon et al., 1999).

The "green" character of methanesulfonic acid (MSA) is a consequence of numerous aspects. In general, the MSA is less toxic than other acids like fluoroboric acid and fluorosilicic acid presenting a reported LD_{50} (oral, rat) of 1158 mg·kg^{-1}. MSA does not have an established OSHA PEL (permissible exposure limit), since MSA solutions (aq), under normal conditions, do not develop any risky volatile chemicals. In general, the low toxicity of MSA, especially when compared with acids of the HF complex makes it a safe electrolyte to control. MSA is easily considered biodegradable eventually developing sulfate and carbon dioxide. In fact, MSA is considered a natural product, being part of the natural sulfur cycle. In general, the harmless character of MSA, especially when compared with other acids, makes it an environmentally advantageous electrolyte (Gernon et al., 1999).

But our main focus is not only to obtain optimized WO_3 nanostructures, but also to study their effectiveness in the photoelectrocatalitic degradation of the pesticide fenamiphos in aqueous solution under irradiation of simulated solar light.

2. MATERIAL AND METHODS.

2.1. WO$_3$ nanostructures fabrication.

WO_3 nanostructures, which will later act as photoanode, were manufactured by the technique known as electrochemical anodization. Prior to this step, the W electrodes were refined by polishing them with 220, 500 and 4000 grain SiC sandpaper, washing them with distilled water and finally drying them with compressed air. The electrodes were then coated with Teflon, leaving exposed only the surface to be anodized. Once the electrode was ready, the anodization was carried out for 4 hours. The conditions that were prefixed were a potential difference of 20 V, a rotation speed of the electrode of 375 rpm (by using a rotating disk electrode, RDE) and a temperature of 50°C and it was used two different electrolytes composed of 1.5 M of H_2SO_4 and 0.05 M of H_2O_2 and another composed by 1.5 M of CH_4O_3S and 0.05 M of H_2O_2. After anodization, fine sections of the electrodes were cut to apply a thermal treatment to the nanostructures for 4 hours at 600°C in an air atmosphere. This last step was carried out to obtain crystalline and dehydrated nanostructures.

2.2. Characterization of the samples.

The obtained nanostructures were characterized by Raman Spectroscopy with a Confocal Raman Laser Microscope (neon laser of 488 nm) to determine their structure and crystal composition. Moreover, they were analyzed morphologically through Field Emission Scanning Electron Microscope (ZEISS ULTRA55 scanning elec-tronmicroscopy) using 2 kV. And finally electrochemically, to investigate the photoelectroactivity of these samples, using experiments under lighting conditions (AM 1.5 conditions at 100 mW·cm^{-2}). In these tests, a quartz cell and three electrodes were used, the nanostructures obtained acting as a photoanode, a platinum mesh as counter electrode and an Ag/AgCl electrode (3 M KCl) as reference electrode. Finally, with an Autolab PGSTAT302N potentiostat, the current values were recorded while applying an external polarization of 1 V.

2.3. Photoelectrocatalytic degradation experiments.

The pesticide used in this study was fenamiphos (Sigma Aldrich Pastanal, analytical standard). Fenamiphos solutions were prepared from a stock solution of 100 mg·L^{-1}, which was stored in a refrigerated atmosphere and in the absence of light. The degradation tests were performed at 20 ° C using the same electrode configuration explained above for the PEIS experiments, applying an external potential difference of 1 V$_{Ag/AgCl}$ to the system and magnetically stirring the electrolyte. Before degradation of the pesticide, this experimental configuration was stirred for 30 minutes in the dark to allow equilibrium of the system. The initial concentration of fenamiphos was 20 mg·L^{-1}, the treated volume was 14 ml and an operating pH of 1 was used, adding the necessary amount of H$_2$SO$_4$.

2.4. Analytical methods

The degradation of the pesticide along the time was controlled by Ultraviolet-Visible spectrophotometry, measuring the absorbance within a range of wavelengths (190-500 nm). Liquid samples of 2 ml were extracted from the quartz reactor every 30 minutes to measure its absorbance. After the measurements, these samples were returned to the reactor to continue the degradation. The degradation tests lasted 360 min. In addition, High-Performance Liquid Chromatography (HPLC) was used for the detection and identification of fenamiphos and its intermediate compounds generated due to the degradation of the pesticide. This analysis was carried out with a Jasco Model PU-2089 pump, equipped with a photodiode array detector MD-2018 Plus and a Kinetex XB-C18 column, 100 × 4.6 mm, with a 2.6 μm particle size and a pore size of 100 Å, using a mobile phase of 40% water/60% methanol and 1 mL·min^{-1} as a flow rate. UV detection of fenamiphos and the intermediate was realized at 254 nm.

3. RESULTS AND DISCUSSION

3.1. Anodization transient

With the aim of studying the formation mechanism of the WO_3 nanostructures used in this work, a current density transient recorded during the 4 h of anodization is presented in Fig. 1. As shown in Fig. 1, in both cases (anodized in H_2SO_4 and in CH_4O_3S) the transient obtained during the anodization is very similar and both have 3 clearly differentiated sections. Just after applying the 20 V, a decrease in the current density is observed which is caused by the formation of a compact layer of WO_3 on the exposed surface of the sample to be anodized. With less exposed surface of tungsten, blocked by the WO_3 film, the current density decreases. The second section corresponds to an increase in current density that is due to the dissolution of the tungsten oxide layer formed in the previous section as a consequence of the reaction between WO_3 and H_2O_2. This dissolution produces in the surface of the tungsten sample a higher exposition and therefore the current density increases. After reaching a maximum value, the current densities decrease again due to the precipitation of tungstic acids from peroxotungstates in the form of nanostructures. This precipitation occurred when supersaturation conditions were reached near the electrode surface (Fernández-Domene et al., 2017).
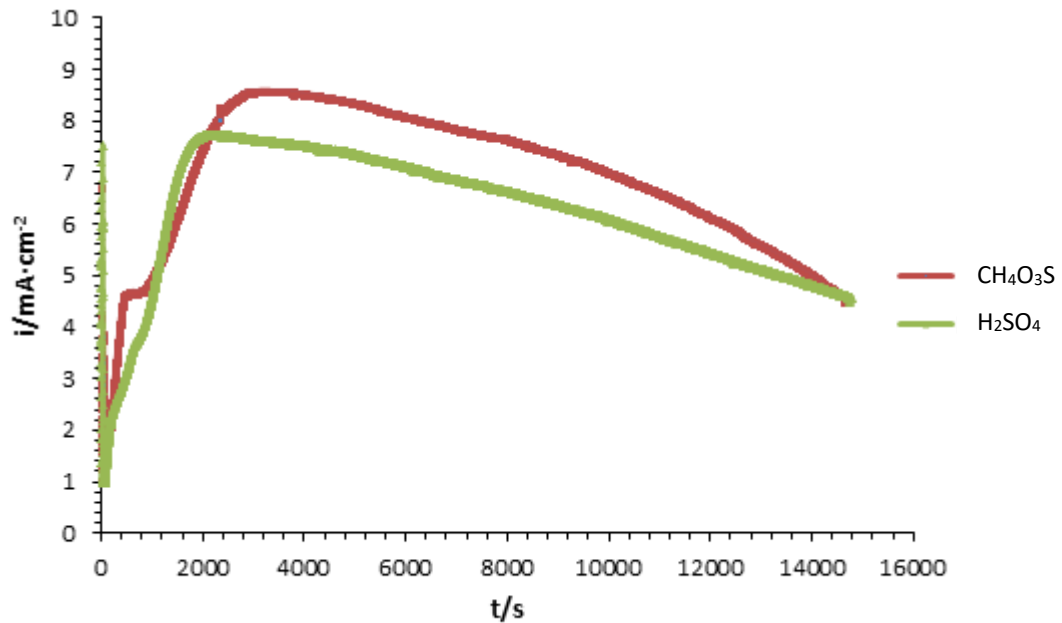

Fig.1. Current density transient recorded during anodization in different electrolytes (1.5 M H_2SO_4 + 0.05 M H_2O_2 and 1.5 M CH_4O_3S + 0.05 M H_2O_2)

3.2. FE-SEM characterization

As explained above in the experimental section, the WO_3 nanostructures were submitted to heat treatment for 4 h to obtain crystalline and dehydrated structures. The morphological characterization of the nanostructures was carried out through FESEM. Fig. 2 shows the morphology of the samples formed in H_2SO_4 electrolyte and in CH_4O_3S electrolyte.
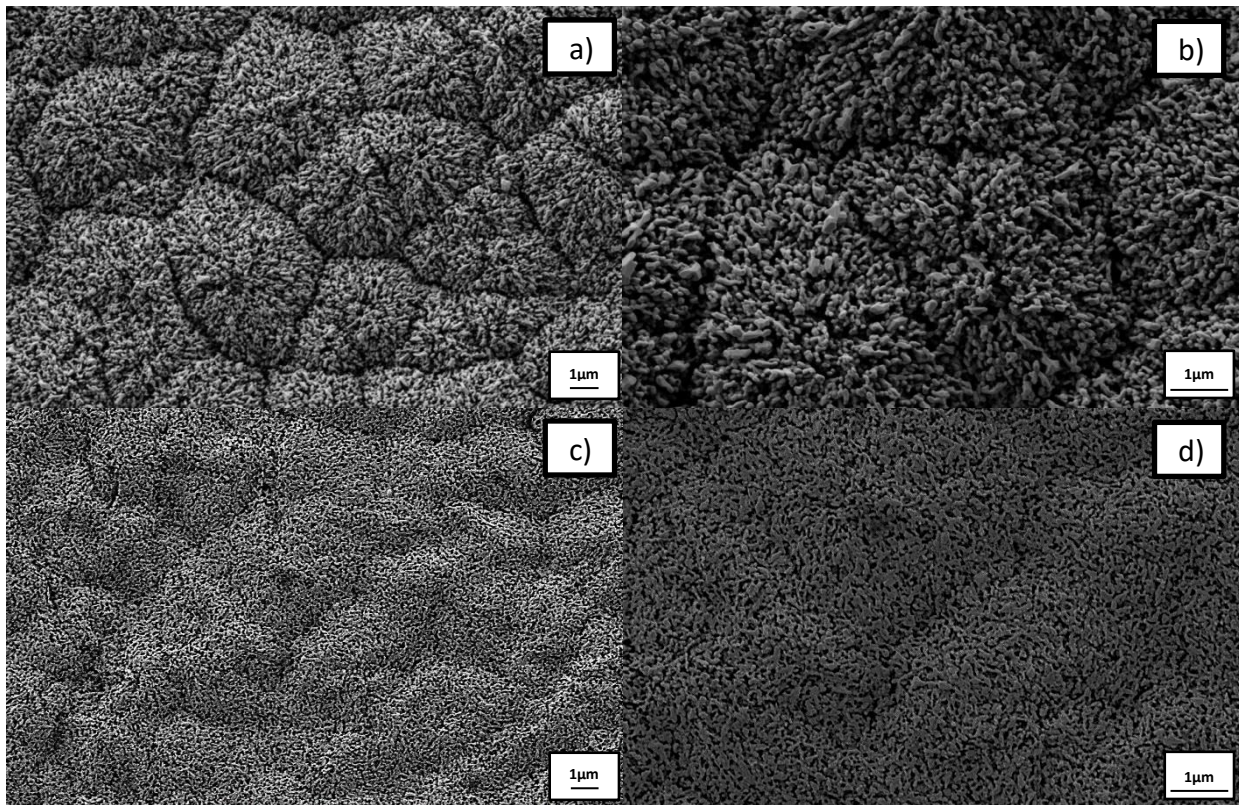
Fig.2. FESEM images of the WO$_3$ nanostructures formed upon anodization of W at 50 °C, imposing a potential of 20 V for 4 h in a) 1.5 M H$_2$SO$_4$ + 0.05 M H$_2$O$_2$ electrolyte at 5000X and b) 1.5 M H$_2$SO$_4$ + 0.05 M H$_2$O$_2$ electrolyte at 10000X, c) 1.5 M CH$_4$O$_3$S+0.05 M H$_2$O$_2$ electrolyte at 5000X and d) 1.5 M CH$_4$O$_3$S+0.05 M H$_2$O$_2$ electrolyte at 10000X.

It could be noticed that in all cases tiny nanorods or nanosheets were obtained on the surface of the electrodes, forming a kind of spongy layer. These nanostructures with such a small size and the way in which they are aggregated may be related to the predisposition of the bidentate O$_2^{2-}$ ligand to establish very strong bonds with tungsten during the experiment, which hindered the growth of the nanostructures during the anodization (Fernández-Domene et al., 2019). However, the acid used as electrolyte during anodization had an effect on the morphology of the nanostructures. With the CH$_4$O$_3$S electrolyte, the nanorods are more compact and more uniform than in case of using H$_2$SO$_4$ as an electrolyte since in the latter case the nanorods are organized in the form of mountains instead of forming a more uniform layer and without alterations as in the case of the CH$_4$O$_3$S. The formation of this more uniform layer, without the presence of nanostructure-free and less porous zones, will result in higher current densities and therefore that nanostructure could be more apt to degrade fenamiphos than nanorods obtained in H$_2$SO$_4$.

3.3. Raman characterization

In order to characterize the composition and crystallinity of the nanostructures Raman Spectroscopy has been used. Fig. 3 shows the Raman spectra after subject the nanostructures to a heat treatment (at 600°C in air atmosphere) in both types of electrolyte. The peaks related to the monoclinic structure of WO_3 are observed in all spectra. The characteristic band of amorphous $WO_3 \cdot xH_2O$ at 950 cm^{-1} does not appear in neither of the two graphs indicating that both nanostructures have transformed from an amorphous structure in the moment of anodization to a crystalline structure after the heat treatment, in addition of being less hydrated (Fernández-Domene et al., 2017). Likewise, the peak observed at 300 cm^{-1} in both spectra indicates that both samples have a high degree of crystallinity (Song et al., 2015). Therefore, with this information, it can be concluded that there are not large differences between both samples and all peaks are indicative of the crystallinity of the samples, in both cases there are dehydrated and crystalline nanostructures (Wang et al., 2013).
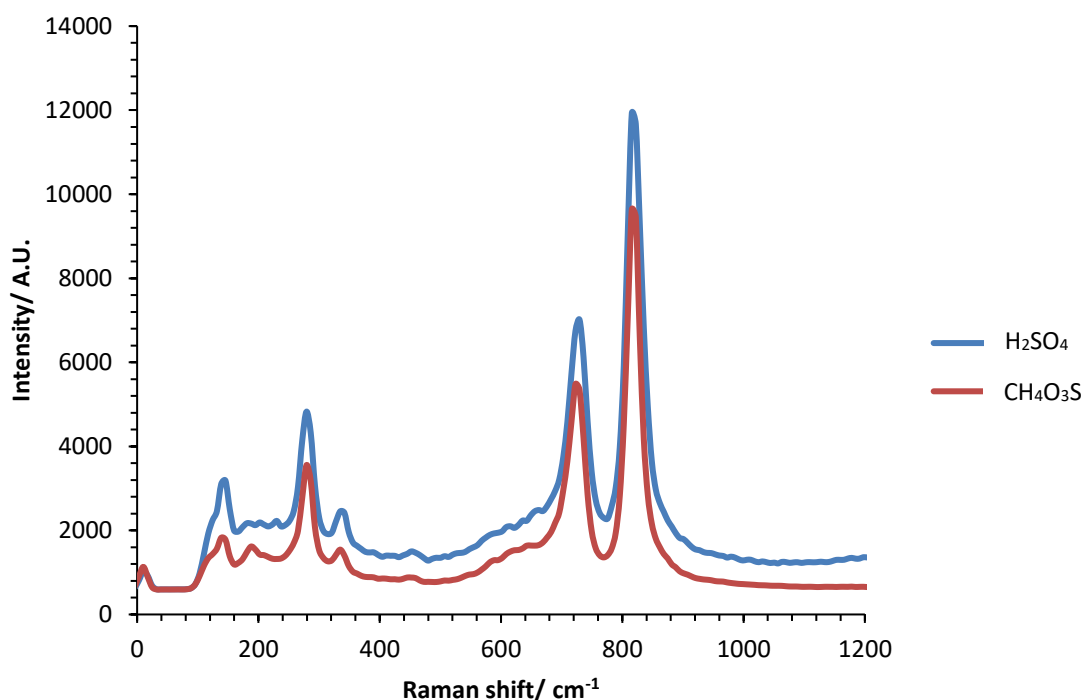

Fig.3. Raman spectra of the samples anodized in the 1.5 M H_2SO_4 + 0.05 M H_2O_2 electrolyte and 1.5 M CH_4O_3S + 0.05 M H_2O_2 electrolyte after the heat treatment at 600°C for 4 h.

3.4. PEIS characterization

In order to test the influence on the charge separation e^-_{CB}/h^+_{VB}, PEIS measurements were carried out under simulated solar light. The photoelectrochemical experiments were performed in a 0.1 M H_2SO_4 solution. Photocurrent densities increase immediately and stay stable under solar radiation in both cases, as observed in Fig.4a. The nanostructures synthesized with CH_4O_3S as electrolyte show the highest

photocurrent response, nearly 0.652 mA·cm^{-2} at 1 V$_{Ag/AgCl}$ in comparison with 0.31 mA·cm^{-2} of H$_2$SO$_4$ as electrolyte. This higher value is associated with the morphology of these nanostructures since the absence of cracks results in a more uniform layer and a greater precipitation of nanostructures, so they exhibit a better photoelectrocatalytic behavior.
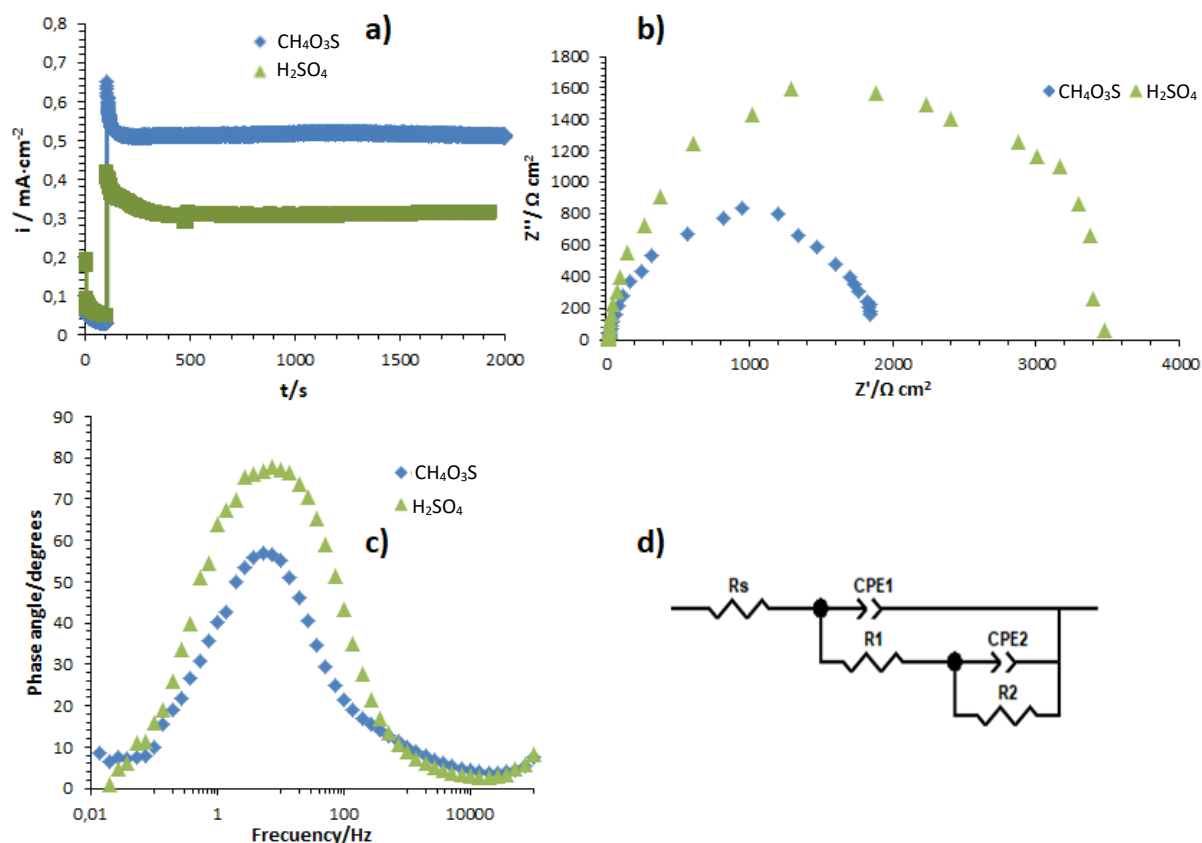

Fig.4. a) Photocurrent density transients obtained under illumination at an applied potential of 1V$_{Ag/AgCl}$ in a 0.1 M H$_2$SO$_4$ solution. b) Nyquist plots, c) Bode-phase plots and d) Equivalent circuit used to fit PEIS data.

Nyquist and Bode-phase plots for the WO$_3$ nanostructures are shown in Fig. 4b and 4c. The Nyquist plots are utilized to study the anode/electrolyte interfaces of the electrode materials and then calculate the charge transfer of holes resistance (Levinas et al., 2017a).

According to Fig. 4b, at first sight one semicircle can be observed in both samples; however at high frequencies appears another semicircle but in this case smaller than the observable. As for the amplitude of the semicircles, the sample synthesized with CH$_4$O$_3$S as electrolyte has smaller amplitude than the other one. This means that charge transfer is favored in this sample more than in the sample synthesized with H$_2$SO$_4$ as electrolyte.

Regarding the Bode plot (Fig. 4c), a peak can be observed in all cases, maybe being an overlap of two different peaks. With CH$_4$O$_3$S as a electrolyte is observed a lower phase

angle which is related with lower impedances (Bertoluzzi and Bisquert, 2012). This concordance is shown in results of this work, so it corroborates that CH_4O_3S presents a better behaviour.

The equivalent circuit is shown in Fig 4d. The R_s is associated with the electrolyte resistance, R_1-CPE_1 with the resistance to the recombination of the electron-hole pairs and R_2-CPE_2 with the charge resistance at the interface electrode-electrolyte. In the circuit, constant phase elements (CPE) have been used instead of capacitors because they simulate the non-ideality of the system.(Kim et al., 2015; Levinas et al., 2017b)

The resistance results of both samples are shown in Table 1, where it can be seen that the sample synthesized with CH_4O_3S as electrolyte presents lower values of resistance to charge transfer and therefore would have a better photoelectrochemical behaviour. These results could be related with the morphology that shows the nanostructures with a better contact between them, which enhanced electrochemical and photoelectrochemical interfacial transference. The results of transient photocurrent and PEIS indicate that nanostructures obtained with CH_4O_3S have the highest separation efficiency of photogenerated charge carries as well as the fastest electronic transport between the electrolyte and nanostructres. Finally, the parameter χ^2 appears to indicate the error made in that setting. It can be seen that χ^2 shows values around the order of 10^{-3} in all cases, which indicated the good adjustment of the experimental data to the proposed theoretical circuit.

Table 1. Resistances values of different experiments.

	H_2SO_4	CH_4O_3S
R_s ($\Omega \cdot cm^2$)	16.52±6	20.39±0.77
R_1 ($\Omega \cdot cm^2$)	26±7	42 ±6.01
R_2 ($k\Omega \cdot cm^2$)	3.48±0.9	1.78±0.38
χ^2	0.0054±0.007	0.0059±0.004

3.5. Photoelectrocatalytic degradation of fenamiphos

Once the optimal nanostructures were determined, degradation tests were carried out. The organophosphorus pesticide to be degraded (fenamiphos, Fig. 5a) was treated by PEC and this process was followed by UV–vis spectrophotometry. Fig. 5b shows the UV–vis absorption spectra for this pesticide (20 mg·L^{-1}), where two well defined bands can be seen, one at 249 nm and a band appearing as a shoulder at 290 nm. The band at 249 nm has been associated with the characteristic fenamiphos aromatic ring $\pi{\rightarrow}\pi^*$ transition where a π electron in a bonding orbital is excited to corresponding anti-bonding orbital π^*. This band is normally used to follow the degradation of this

pesticide whereas the shoulder corresponds to n– π* transition concerning the sulfur atom where an electron from non-bonding orbital is promoted to anti-bonding π* orbital (Tajeddine et al., 2010).
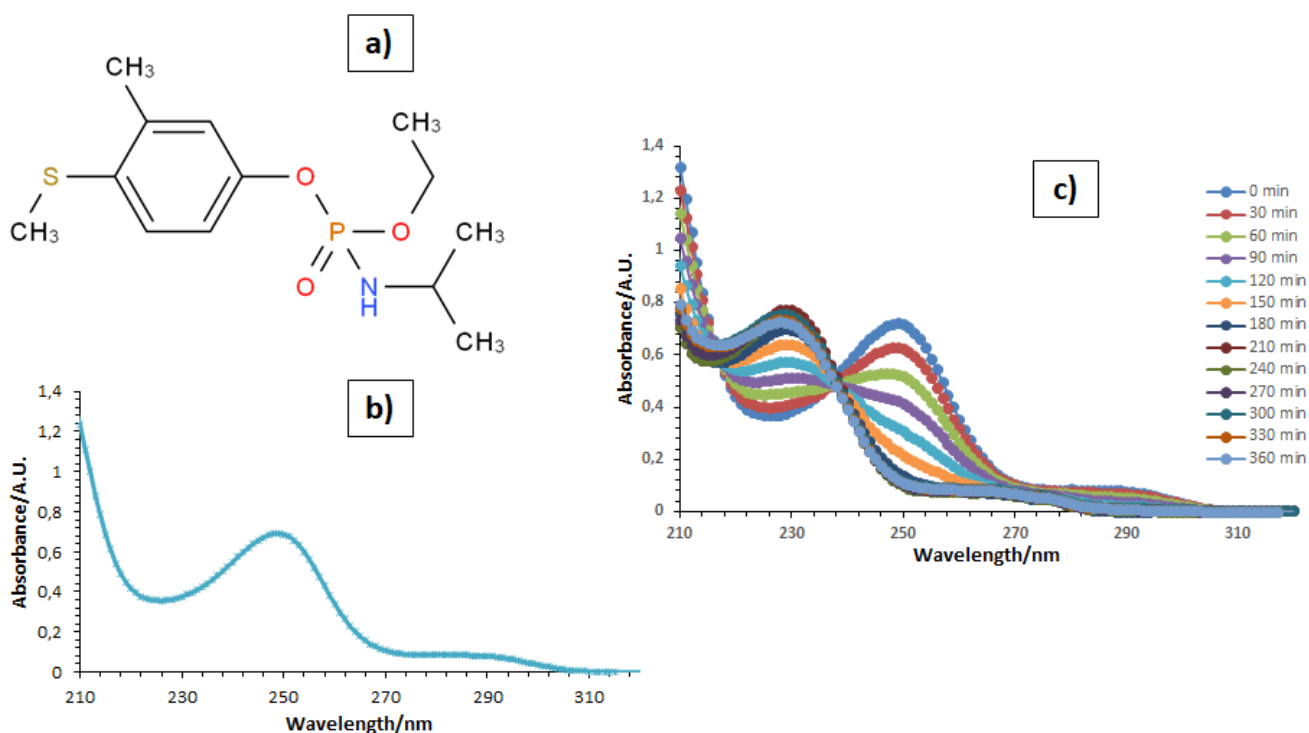

Fig.5a) Fenamiphos molecule, b) UV–Vis spectra of fenamiphos at 20 mg·L^{-1}, c) Fenamiphos UV–Vis spectra when PEC technique is used during 6 hours.

In Fig. 5c, the evolution of UV-Vis spectra of the pesticide is shown during the 6 hours of degradation (sample was taken every half hour). As it can be seen, the band at 249 nm and the small shoulder registered at 290 nm decrease over time until practically disappearing. However, at 229 nm it is observed that with the pass of time a new band appears, which corresponds to a degradation intermediate that is being formed, but this band decreases a little with time at the end of the test. This degradation intermediate may correspond to a breakdown of the pesticide molecule through ethanothiol bond or phosphoramidate bond (Sogorb et al., 2002), resulting in a smaller and less polar molecule. This would be the reason why the peak appears to the left, at shorter wavelengths, since both ethanothiol and phosphoramidate bond act as auxochromes. The auxochromes are the functional groups attached to the chromophores (they are the part of the molecule responsible for imparting color or the functional groups that contain multiple bonds capable of absorbing radiation above 200 nm due to the transitions π → π* and n– π*) that modify their ability to absorb light, altering the wavelength or absorption intensity towards longer wavelengths. Therefore, the intermediate band appears at lower wavelengths (λ) than the main band of fenamiphos, since this intermediate has lost the auxochromes (one or both of the auxochromes) that confer that increase in the recorded wavelength ("IARC monographs on the evaluation of carcinogenic risks to humans," 2010).

In addition, with the new band at 229 nm, a point called isosbestic appears (it is represented by an asterisk in Fig. 5c). The appearance of these points are observed in overlapped spectra when a chromophoric reagent is transformed to a product with a different spectrum, so that it is frequently supposed that an isosbestic point happens only when the reagent is quantitatively transformed to a single product (Berlett et al., 2000). According to this definition, it can be affirmed that during the degradation only one chemical reaction occurred and therefore only one degradation intermediate was obtained.

Then, by HPLC measurements, the standards and the pesticide samples taken every hour were analyzed. First of all, the standards were measured to create a calibration line (eq. 1) which will be used to find the concentration of fenamiphos in the samples.

$$Area = 23026 \cdot C(t) \qquad eq.1$$

Fig. 6 shows the HPLC chromatograms of fenamiphos and its intermediate recorded at different reaction times. In these chromatograms it can be seen that after two hours all the pesticide had been degraded since the peak that appears at a retention time (t_R) of 1.96 min (which corresponds to fenamiphos) disappears after 2 hours. From the calibration line obtained, the concentration of fenamiphos present in all samples is calculated. In the sample taken at 1 hour the area registered was 139098 and, therefore, the concentration present in the sample was 6.04 mg·L^{-1}. For the sample taken at 2 hours the area obtained was 7390 which corresponds to a concentration of 0.32 mg·L^{-1}. So, it can be concluded that at 2 hours fenamiphos has been completely degraded and in the following samples there is no presence of the pesticide.

In addition, in Fig. 6 a new peak can also be observed at a lower retention time (t_R 1.3 min) which corresponds to the degradation intermediate. However, this peak after 3 hours of degradation begins to decrease since the correspondent compound is also degraded. All this agrees with the UV-Vis spectrum since both the HPLC and the UV-Vis show the appearance and subsequent disappearance of the peak corresponding to the degradation intermediate, which presents a clear absorption band at 229 nm.
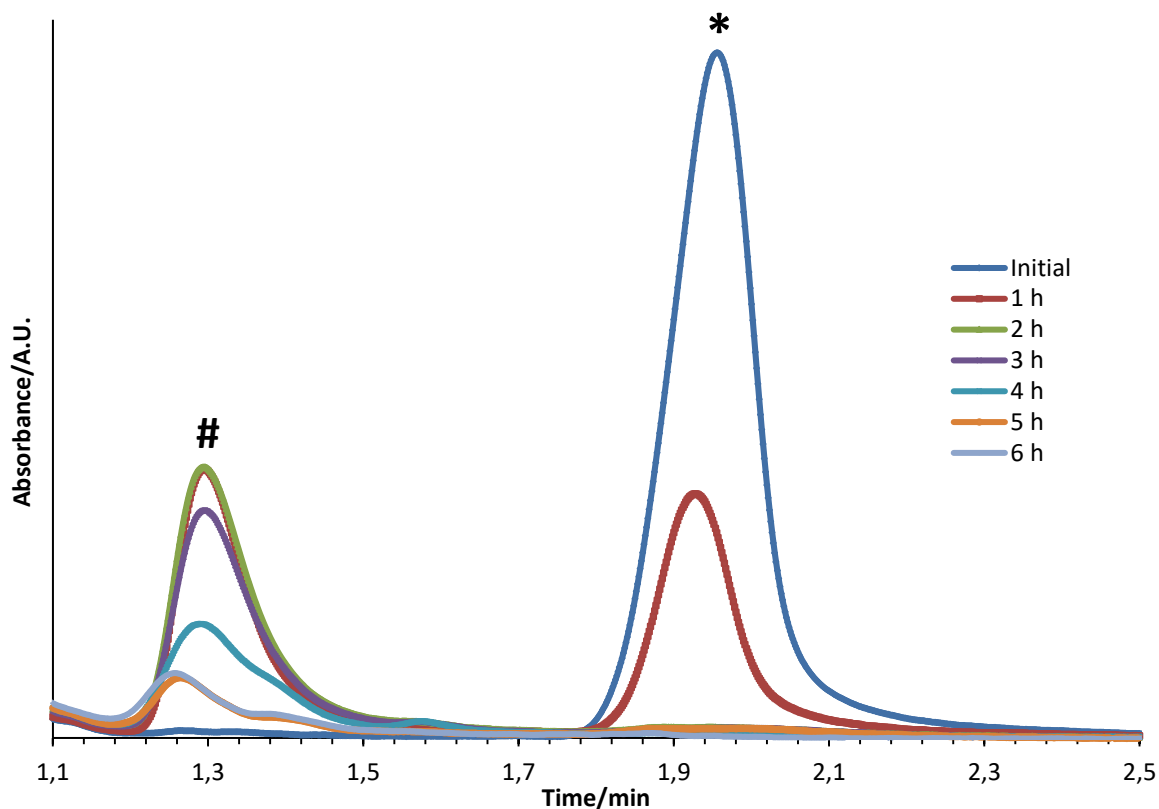
Fig.6) HPLC chromatograms of fenamiphos and its intermediate recorded at different reaction times where peak with * correspond to fenamiphos and peak with # correspond to its intermediate.

In order to finalize the analysis and comparison of the results obtained with all methods, it can be concluded that the band recorded at 249 nm does not drop radically in the UV-Vis spectrum at two hours because the degradation intermediate also absorbs at that wavelength, like the intermediate spectra of Fig. S2 shows. Moreover, as seen in Fig. 6, the peak corresponding to the intermediate (t_r=1.3 min) is decreasing until almost disappearing, therefore this may be due to the subsequent degradation of the intermediate when the rupture of aromatic ring takes place.

4. CONCLUSIONS

In summary, WO$_3$ nanostructures have been satisfactorily obtained by varying the acid electrolyte to optimize the nanostructures behaviour. All the samples have been morphologically analyzed by FESEM, their composition and crystallinity has been studied through Raman and their photoelectrochemical behaviour through PEIS. The optimal nanostructures were obtained with 1.5 M CH$_4$O$_3$S + 0.05 M H$_2$O$_2$, since they showed better morphological and photoelectrochemical properties such as a higher photocurrent density and a lower charge transfer resistance.

Regarding to the results obtained about fenamiphos degradation with UV-Vis spectra and using HPLC technique, it can be concluded that the pesticide was degraded quicker

than the UV-Vis spectra showed, after two hours a 100% of degradation was achieved. Furthermore, a degradation intermediate was formed during the PEC process but after three hours it began to being degraded too. The fenamiphos degradation path would include the formation of a single intermediate, according to the isosbestic point observed in the UV-Vis spectrum, which could be formed due to the breakage of the ethanothiol bond and/or the phosphoramidate bond to give a smaller molecule producing a degradation intermediate that absorbs at shorter wavelengths. In subsequent steps, this intermediate underwent further degradation probably due to the opening of the aromatic ring.

Acknowledgments

REFERENCES:

Bamwenda, G.R., Sayama, K., Arakawa, H., 1999. The effect of selected reaction parameters on the photoproduction of oxygen and hydrogen from a WO3-Fe2+-Fe3+ aqueous suspension. J. Photochem. Photobiol. A Chem. 122, 175–183. https://doi.org/10.1016/S1010-6030(99)00026-X

Berger, S., Tsuchiya, H., Ghicov, A., Schmuki, P., 2006. High photocurrent conversion efficiency in self-organized porous WO 3. Appl. Phys. Lett. 88, 88–91. https://doi.org/10.1063/1.2206696

Berlett, B.S., Levine, R.L., Stadtman, E.R., 2000. Use of isosbestic point wavelength shifts to estimate the fraction of a precursor that is converted to a given product. Anal. Biochem. 287, 329–333. https://doi.org/10.1006/abio.2000.4876

Bertoluzzi, L., Bisquert, J., 2012. Equivalent circuit of electrons and holes in thin semiconductor films for photoelectrochemical water splitting applications. J. Phys. Chem. Lett. 3, 2517–2522. https://doi.org/10.1021/jz3010909

Budd, W.W., Young, G.L., 2006. Environmental science. Environ. Geol. 5, 224–224. https://doi.org/10.1007/1-4020-4494-1_124

Cáceres, T., Megharaj, M., Naidu, R., 2008. Degradation of fenamiphos in soils collected from different geographical regions: The influence of soil properties and climatic conditions. J. Environ. Sci. Heal. - Part B Pestic. Food Contam. Agric. Wastes 43, 314–322. https://doi.org/10.1080/03601230801941659

Cáceres, T., Megharaj, M., Venkateswarlu, K., Sethunathan, N., Naidu, R., 2010. Fenamiphos and Related Organophosphorus Pesticides : Environmental Fate and Toxicology. https://doi.org/10.1007/978-1-4419-5623-1

Chakrapani, V., Thangala, J., Sunkara, M.K., 2009. WO 3 and W 2 N nanowire arrays for photoelectrochemical hydrogen production. Int. J. Hydrogen Energy 34, 9050–9059. https://doi.org/10.1016/j.ijhydene.2009.09.031

Chen, S., Sun, D., Chung, J.S., 2007. Treatment of pesticide wastewater by moving-bed biofilm reactor combined with Fenton-coagulation pretreatment. J. Hazard. Mater. 144, 577–584. https://doi.org/10.1016/j.jhazmat.2006.10.075

Cycoń, M., Zmijowska, A., Wójcik, M., Piotrowska-Seget, Z., 2013. Biodegradation and bioremediation potential of diazinon-degrading Serratia marcescens to remove other organophosphorus pesticides from soils. J. Environ. Manage. 117, 7–16. https://doi.org/10.1016/j.jenvman.2012.12.031

Daghrir, R., Drogui, P., Robert, D., 2012. Photoelectrocatalytic technologies for environmental applications. J. Photochem. Photobiol. A Chem. 238, 41–52. https://doi.org/10.1016/j.jphotochem.2012.04.009

Enesca, A., Duta, A., Schoonman, J., 2007. Study of photoactivity of tungsten trioxide (WO3) for water splitting. Thin Solid Films 515, 6371–6374. https://doi.org/10.1016/j.tsf.2006.11.135

Fernández-Domene, R.M., Roselló-Márquez, G., Sánchez-Tovar, R., Lucas-Granados, B., García-Antón, J., 2019. Photoelectrochemical removal of chlorfenvinphos by using WO3 nanorods: Influence of annealing temperature and operation pH. Sep. Purif. Technol. 212, 458–464. https://doi.org/10.1016/j.seppur.2018.11.049

Fernández-Domene, R.M., Sánchez-Tovar, R., Lucas-Granados, B., Roselló-Márquez, G., García-Antón, J., 2017. A simple method to fabricate high-performance nanostructured WO3 photocatalysts with adjusted morphology in the presence of complexing agents. Mater. Des. 116, 160–170. https://doi.org/10.1016/j.matdes.2016.12.016

Fraga, L.E., Franco, J.H., Orlandi, M.O., Zanoni, M.V.B., 2013. Photoelectrocatalytic oxidation of hair dye basic red 51 at W/WO 3/TiO2 bicomposite photoanode activated by ultraviolet and visible radiation. J. Environ. Chem. Eng. 1, 194–199. https://doi.org/10.1016/j.jece.2013.04.018

Georgieva, J., Sotiropoulos, S., Armyanov, S., Philippidis, N., Poulios, I., 2011. Photoelectrocatalytic activity of bi-layer TiO2/WO3 coatings for the degradation of 4-chlorophenol: Effect of morphology and catalyst loading. J. Appl. Electrochem. 41, 173–181. https://doi.org/10.1007/s10800-010-0221-8

Gernon, M.D., Wu, M., Buszta, T., Janney, P., 1999. Environmental benefits of methanesulfonic acid. Green Chem. 1, 127–140. https://doi.org/10.1039/a900157c

Ghaemi, N., Madaeni, S.S., Alizadeh, A., Rajabi, H., Daraei, P., 2011. Preparation, characterization and performance of polyethersulfone/organically modified montmorillonite nanocomposite membranes in removal of pesticides. J. Memb. Sci. 382, 135–147. https://doi.org/10.1016/j.memsci.2011.08.004

Golash, N., Gogate, P.R., 2012. Degradation of dichlorvos containing wastewaters using sonochemical reactors. Ultrason. Sonochem. 19, 1051–1060.

https://doi.org/10.1016/j.ultsonch.2012.02.011

Guo, Y., Quan, X., Lu, N., Zhao, H., Chen, S., 2007. High photocatalytic capability of self-assembled nanoporous WO3 with preferential orientation of (002) planes. Environ. Sci. Technol. 41, 4422–4427. https://doi.org/10.1021/es062546c

He, T., Yao, J., 2007. Photochromic materials based on tungsten oxide. J. Mater. Chem. 17, 4547–4557. https://doi.org/10.1039/b709380b

Helbling, D.E., 2015. Bioremediation of pesticide-contaminated water resources: The challenge of low concentrations. Curr. Opin. Biotechnol. 33, 142–148. https://doi.org/10.1016/j.copbio.2015.02.012

IARC monographs on the evaluation of carcinogenic risks to humans, 2010. . IARC Monogr. Eval. Carcinog. Risks to Humans 93, 9–38.

Kidd, H. and James, D. R., 1991. The agrochemicals handbook, Third edit. ed, Agriculture, Ecosystems & Environment. Royal Society of Chemistrysociety of Chemestry, Cambridge, U.K.

Kim, Y.O., Yu, S.H., Ahn, K.S., Lee, S.K., Kang, S.H., 2015. Enhancing the photoresponse of electrodeposited WO3 film: Structure and thickness effect. J. Electroanal. Chem. 752, 25–32. https://doi.org/10.1016/j.jelechem.2015.05.031

Levinas, R., Tsyntsaru, N., Lelis, M., Cesiulis, H., 2017a. Synthesis, electrochemical impedance spectroscopy study and photoelectrochemical behaviour of as-deposited and annealed WO3 films. Electrochim. Acta 225, 29–38. https://doi.org/10.1016/j.electacta.2016.12.112

Levinas, R., Tsyntsaru, N., Lelis, M., Cesiulis, H., 2017b. Synthesis, electrochemical impedance spectroscopy study and photoelectrochemical behaviour of as-deposited and annealed WO3 films. Electrochim. Acta 225, 29–38. https://doi.org/10.1016/j.electacta.2016.12.112

Li, W., Li, J., Wang, X., Ma, J., Chen, Q., 2010. Photoelectrochemical and physical properties of WO 3 films obtained by the polymeric precursor method. Int. J. Hydrogen Energy 35, 13137–13145. https://doi.org/10.1016/j.ijhydene.2010.09.011

Liu, Y., Ohko, Y., Zhang, R., Yang, Y., Zhang, Z., 2010. Degradation of malachite green on Pd/WO3 photocatalysts under simulated solar light. J. Hazard. Mater. 184, 386–391. https://doi.org/10.1016/j.jhazmat.2010.08.047

Liu, Y., Xie, C., Li, H., Chen, H., Liao, Y., Zeng, D., 2011. Low bias photoelectrocatalytic (PEC) performance for organic vapour degradation using TiO2/WO3 nanocomposite. Appl. Catal. B Environ. 102, 157–162. https://doi.org/10.1016/j.apcatb.2010.11.037

Maldonado, M.I., Passarinho, P.C., Oller, I., Gernjak, W., Fernández, P., Blanco, J., Malato, S., 2007. Photocatalytic degradation of EU priority substances: A comparison between TiO 2 and Fenton plus photo-Fenton in a solar pilot plant. J. Photochem. Photobiol. A Chem. 185, 354–363. https://doi.org/10.1016/j.jphotochem.2006.06.036

Mehta, R., Brahmbhatt, H., Saha, N.K., Bhattacharya, A., 2015. Removal of substituted phenyl urea pesticides by reverse osmosis membranes: Laboratory scale study for field water application. Desalination 358, 69–75. https://doi.org/10.1016/j.desal.2014.12.019

Michael. A. Kamrin, 2010. Pesticides Profile (Toxicity, Environmental Impact, and Fate), Resticides Profiles (Toxicity, Enviromental Impact and Fate. CRC Press LLC, Michigan.

Miller, E.L., Marsen, B., Cole, B., Lum, M., 2006. Low-Temperature Reactively Sputtered Tungsten Oxide Films for Solar-Powered Water Splitting Applications. Electrochem. Solid-State Lett. 9, G248. https://doi.org/10.1149/1.2201994

Moussavi, G., Hosseini, H., Alahabadi, A., 2013. The investigation of diazinon pesticide removal from contaminated water by adsorption onto NH4Cl-induced activated carbon. Chem. Eng. J. 214, 172–179. https://doi.org/10.1016/j.cej.2012.10.034

Navarro, S., Fenoll, J., Vela, N., Ruiz, E., Navarro, G., 2009. Photocatalytic degradation of eight pesticides in leaching water by use of ZnO under natural sunlight. J. Hazard. Mater. 172, 1303–1310. https://doi.org/10.1016/j.jhazmat.2009.07.137

Ou, L.-T., Thomas, J.E., Dickson, D.W., 2010. Degradation of Fenamiphos in Soil with a History of Continuous Fenamiphos Applications. Soil Sci. Soc. Am. J. 58, 1139. https://doi.org/10.2136/sssaj1994.03615995005800040019x

Paul, B., Martens, W.N., Frost, R.L., 2012. Immobilised anatase on clay mineral particles as a photocatalyst for herbicides degradation. Appl. Clay Sci. 57, 49–54. https://doi.org/10.1016/j.clay.2011.12.009

Plakas, K. V., Karabelas, A.J., 2012. Removal of pesticides from water by NF and RO membranes - A review. Desalination 287, 255–265. https://doi.org/10.1016/j.desal.2011.08.003

Rass-Hansen, J., Falsig, H., Jørgensen, B., Christensen, C.H., 2007. Perspective Bioethanol: fuel or feedstock. J. ofChemical Technol. Biotechnol. 82, 329–333. https://doi.org/10.1002/jctb

Reddy, P.V.L., Kim, K.H., 2015. A review of photochemical approaches for the treatment of a wide range of pesticides. J. Hazard. Mater. 285, 325–335. https://doi.org/10.1016/j.jhazmat.2014.11.036

Saini, R., Kumar, P., 2016. Journal of Environmental Chemical Engineering Simultaneous removal of methyl parathion and chlorpyrifos pesticides from model wastewater using coagulation / fl occulation : Central composite design. Biochem. Pharmacol. 4, 673–680. https://doi.org/10.1016/j.jece.2015.12.020

Santato, C., Odziemkowski, M., Ulmann, M., Augustynski, J., 2001. Crystallographically oriented mesoporous WO3 films: Synthesis, characterization, and applications. J. Am. Chem. Soc. 123, 10639–10649. https://doi.org/10.1021/ja011315x

Sarkar, B., Venkateswralu, N., Rao, R.N., Bhattacharjee, C., Kale, V., 2007. Treatment of pesticide contaminated surface water for production of potable water by a coagulation-adsorption-nanofiltration approach. Desalination 212, 129–140. https://doi.org/10.1016/j.desal.2006.09.021

Singh, B.K., Walker, A., 2006. Microbial degradation of organophosphorus compounds. FEMS Microbiol. Rev. 30, 428–471. https://doi.org/10.1111/j.1574-6976.2006.00018.x

Sogorb, M.A., Monroy-Noyola, A., Vilanova, E., 2002. Importancia de la hidrolisis estereoespecifica en la evaluacion de riesgos toxicos de insecticidas fosforamidatos. Rev. Toxicol. 19, 61–67.

Song, H., Li, Y., Lou, Z., Xiao, M., Hu, L., Ye, Z., Zhu, L., 2015. Synthesis of Fe-doped WO3 nanostructures with high visible-light-driven photocatalytic activities. Appl. Catal. B Environ. 166–167, 112–120. https://doi.org/10.1016/j.apcatb.2014.11.020

Tajeddine, L., Nemmaoui, M., Mountacer, H., Dahchour, A., Sarakha, M., 2010. Photodegradation of fenamiphos on the surface of clays and soils. Environ. Chem. Lett. 8, 123–128. https://doi.org/10.1007/s10311-008-0198-2

Tsuchiya, H., Macak, J.M., Sieber, I., Taveira, L., Ghicov, A., Sirotna, K., Schmuki, P., 2005. Self-organized porous WO3 formed in NaF electrolytes. Electrochem. commun. 7, 295–298. https://doi.org/10.1016/j.elecom.2005.01.003

Vukčević, M.M., Kalijadis, A.M., Vasiljević, T.M., Babić, B.M., Laušević, Z. V., Laušević, M.D., 2015. Production of activated carbon derived from waste hemp (Cannabis sativa) fibers and its performance in pesticide adsorption. Microporous Mesoporous Mater. 214, 156–165. https://doi.org/10.1016/j.micromeso.2015.05.012

Wang, C.K., Lin, C.K., Wu, C.L., Wang, S.C., Huang, J.L., 2013. Synthesis and characterization of electrochromic plate-like tungsten oxide films by acidic treatment of electrochemical anodized tungsten. Electrochim. Acta 112, 24–31. https://doi.org/10.1016/j.electacta.2013.07.204

Watcharenwong, A., Chanmanee, W., de Tacconi, N.R., Chenthamarakshan, C.R., Kajitvichyanukul, P., Rajeshwar, K., 2008. Anodic growth of nanoporous WO3 films: Morphology, photoelectrochemical response and photocatalytic activity for methylene blue and hexavalent chrome conversion. J. Electroanal. Chem. 612, 112–120. https://doi.org/10.1016/j.jelechem.2007.09.030

Xiao, F.X., Miao, J., Tao, H.B., Hung, S.F., Wang, H.Y., Yang, H. Bin, Chen, J., Chen, R., Liu, B., 2015. One-dimensional hybrid nanostructures for heterogeneous photocatalysis and photoelectrocatalysis. Small 11, 2115–2131. https://doi.org/10.1002/smll.201402420

Yang, C., Zeng, Q., Yang, Y., Xiao, R., Wang, Y., Shi, H., 2014. The synthesis of humic acids graft copolymer and its adsorption for organic pesticides. J. Ind. Eng. Chem. 20, 1133–1139. https://doi.org/10.1016/j.jiec.2013.07.001

Zheng, H., Tachibana, Y., Kalantar-Zadeh, K., 2010. Dye-sensitized solar cells based on WO3. Langmuir 26, 19148–19152. https://doi.org/10.1021/la103692y

Zhou, J., Ding, Y., Deng, S.Z., Gong, L., Xu, N.S., Wang, Z.L., 2005. Three-dimensional tungsten oxide nanowire networks. Adv. Mater. 17, 2107–2110. https://doi.org/10.1002/adma.200500885